Experimental characterization of an anode-supported tubular SOFC generator fueled with hydrogen, including a principal component analysis and a multi-linear regression

Published in: International journal of hydrogen energy, Vol. 36, No. 14, 07.2011, p. 8435-8449.

Experimental characterization of an anode-supported tubular SOFC generator fueled with hydrogen, including a principal component analysis and a multi-linear regression

G. Santori, E. Brunetti, F. Polonara

Abstract

Solid oxide fuel cell (SOFC) power generators can now be commercialized as heat and power micro-cogenerator. Few well-documented field tests have been conducted to date on these units' tubular cell architecture, however, and little has been done to derive general rules for a thorough understanding of these units' operation. The present work focuses on characterizing the hydrogen-powered Acumentrics Gen521 (rated 2.5 kW) under various stable conditions. A test rig was installed at the Dipartimento di Energetica of the Università Politecnica delle Marche (Ancona, Italy) to ascertain the main characteristic curves of the Acumentrics Gen521. A multivariate data analysis was performed on the experimental data collected to establish the operating parameters most influential for the stack voltage (SV) and the DC stack output power generated in different working conditions. Some multi-linear response surfaces are suggested for predicting the SV and the DC power in different operating conditions.

Key words: SOFC, experimental test, tubular fuel cells, power generation, performance analysis, linear regression.

1. Introduction

Solid oxide fuel cell (SOFC) power generation systems have been intensively developed and these machines are now nearly ready for commercialization. There are still few reports of field tests on these units [1-5]**,** while in the last two decades researchers have been especially active in developing mathematical models [6-12] and the results of this research activity point to several issues open to further investigations:

1. the heat, mass and charge transport in single cells and stacks still require in-depth study [13];
2. only a few of published mathematical models have undergone experimental validation;
3. the thermophysical properties and reaction kinetics of several materials at high temperatures are still not well known [14-17].

The experimental activities conducted on SOFCs have been characterized mainly by: (i) the study of new materials [18]; (ii) developments in single cell design [19-21]; (iii) the development of cell manufacturing methods, with numerous studies on the parameters that influence the microstructure of the materials [20-23]. As a result, the open literature is still short of information on the validation of the generation system's performance as a whole.

The documented tests to date on SOFC generators focused on: a) durability under stressing; b) long-term life; c) performance. Such tests have been conducted on the following units:

1) Sulzer Hexis HXS 1000 (1kWel) [1]: this unit is fueled with natural gas. It uses a planar geometry and can provide 1 kWel and 24.5kWth by means of an auxiliary boiler. The experimental campaign was started in March 2002, but so far no results have been circulated about the commercial unit;

2) Siemens CHP-100 SOFC Field Unit, also named EDB/ELSAM 100 (100 kWel) [2]: this unit consists of Siemens-designed tubular cells fed with natural gas. It has been in operation for 36900 hours and submitted to tests on its durability and performance, reaching an electrical efficiency (AC) of 40.07% and a global (electrical and thermal) efficiency of

61.10%. An analysis of variance (ANOVA) was conducted on the voltage considering as parameters the mean temperature of the stack and the utilization factor.
3) Siemens SFC 5 Alpha 6 (3.5 kWel) [3]: this unit is fueled with natural gas and has Siemens-designed tubular cells. Tests have been performed on its performance, obtaining an electrical efficiency (AC) of 35.50% and a global efficiency of 65.32%. Here again, an ANOVA was conducted on the voltage considering as parameters the mean temperature of the stack and the utilization factor.
4) Siemens SCE 220kW (220kWel) [4]: this unit has the same features of the stack as the EDB/ELSAM 100. The unit was tested at 3 atm. The reported data indicate that the unit worked for 3000 hours and was then switched off. The unit had been designed to run coupled with a gas turbine.
5) Acumentrics CP-SOFC 5000 (5 kWel) [5]: this unit consists of Acumentrics-designed tubular solid oxide cells. Durability tests have been performed and the unit has been operated for 1500 hours. Some aspects of its performance have been classified, as concerns the reduction in the average manifold voltage time. The machine was submitted to three stops and starts as a stressing test.
The tests conducted therefore focused mainly on durability, while few systematic studies have attempted to derive fundamental rules on these units' operation.
Concentrating now exclusively on the performance testing activities, a thorough description of experiments conducted on a large SOFC generator is given in [19], where a detailed statistical analysis is provided, also based on the experimental design proposed. Using this method enables important conclusions to be drawn on the operation of the system with variations in the utilization factor and the air flow delivered to the SOFC generator. On the other hand, the proposed method makes it difficult to select a considerable number of parameters to vary because the machine takes effect on many of them on the strength of its internal control logic, thereby restricting the conclusions that can be drawn.
The problem of deducing general rules derives from the way in which the data collected are presented, which is typically in arrays of time-dependent values. This means that, when the operating variables are graphed in relation to one another, instead of evident trends, simply clusters of points are obtained in certain areas representing different operating conditions.
The unit may then be characterized by taking three interpretative approaches: (i) by solving the equations of energy and momentum conservation, coupled with a formula for estimating the chemical species involved in the electrochemical reaction [20]; (ii) by treating the SOFC generator as a gray box [21]; or (iii) as a black box.
By treating the unit as a black box, this paper proposes a new approach to quantifying the performance of the 2.5kWel generator by Acumentrics (Gen521), fueled with hydrogen produced by water electrolysis, in terms of stack voltage (SV) and DC electrical power in various operating conditions.
Adopting a multivariate method to analyze the data enables data to be derived in order to interpret the system as a black box. Various response surfaces can be used to predict the SV and the DC power in different working conditions and using exclusively input-output data.
Multivariate methods of data analysis are now commonly used to characterize biological and environmental systems [22-24], but their application to the characterization of fuel cell systems is still relatively rare [25, 26]. In particular a recent application of a multivariate data analysis named principal component analysis (PCA) to PEM fuel cells is documented in [27]. As shown in [28] the relations derived by this method could be implemented on control devices of a fuel cell generator instead of the presently-adopted proportional-integral systems. The PCA also reveals the most crucial operational aspects, identifying the parameters that most influence the unit's performance. This data analysis is particularly useful when performance depends on a large number of parameters, as in [27] for instance, where 62

parameters were adopted and it was necessary to simplify the study considering exclusively the most important operating parameters.
In the present case, the SOFC generator's performance depends on the interactions between some of its sections. The constitutive elements of a SOFC generator are the balance of plant (BoP), the power conditioning system (PCS), the fuel cell stack, and the electronic control and monitoring system. In fact, the control of the electrochemical reaction in the stack gives rise to the optimal thermodynamic conditions for each electrical load required, but in this condition the PCS might operate at the point of minimum efficiency, reducing the electrical power generated. The control loops in the control and monitoring system may also not always be set correctly when the unit operates under variable electrical loads [29], giving rise to further inefficiencies.
The results of operating SOFC generators therefore still fall far short of the performance achievable with other more efficient power generation systems. However, the advantage of a SOFC generator lies in its ability to maintain the same performance over a wide range of rated electrical power making it suitable for distributed generation. The performance characterization of the Gen521 is outlined below, based on data obtained from an experimental campaign processed using PCA. The data analysis also highlights how the machine's various operating parameters influence the performance in different working conditions. Finally, the data were used to develop simple but sufficiently accurate equations (taking the black box approach) capable of defining the behavior of the Gen521.

2. The test rig

An outdoor test rig was set up to quantify the performance of the Gen521 (Figure 1) at the Dipartimento di Energetica of Università Politecnica delle Marche (Ancona, Italy). The test rig comprises:
- a water demineralization unit with a storage container: the amount of demineralized water needed for hydrogen production is about 0.00083 l/s. The water must be demineralized to prevent the electrolyte's deactivation. The maximum effective demineralized water production is 0.0012 l/s. The resulting purified water that is not used is stored in a 50-liter tank;
- an electrolyzer, using NaOH as the electrolyte and separately producing hydrogen and oxygen. The maximum flow rate at ambient conditions is 1.22 l/s of hydrogen with a purity varying between 99.3% and 99.8%. The unit's maximum pressure at the hydrogen outlet is 4 bar. Hydrogen and oxygen are produced and stored in two separate tanks inside the electrolyzer at 2.8 bar and 60°C. The electrolyzer's maximum electrical power absorption is 23 kW;
- a drying column: the hydrogen is dried in a hydrophilic granular salt bed ($CaCl_2$);
- the Acumentrics Gen521 atmospheric SOFC generator;
- a series of AC electrical loads consisting of 5 individual lights.

A control, monitoring and data acquisition system was developed by Acumentrics Corp. to characterize the SOFC generator. The software was implemented in C language with a LabVIEW 6.1 interface. Figure 2 shows the position of the measuring devices in the SOFC machine under investigation. The voltage sensors installed provide the difference in potential between two tubes belonging to a manifold. In addition to the sensors connected to the generator, several electrolyzer parameters are also measured. Table 1 shows the main characteristics of the sensors involved in the installation.

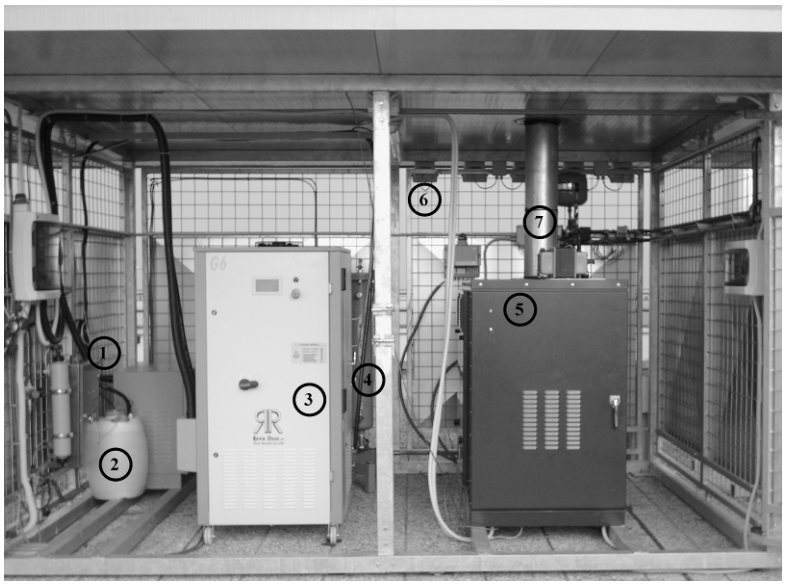

Figure 1. Test rig. 1. Demineralization unit 2. Demineralized water tank 3. Electrolyzer 4. Drying bed 5. Acumentrics Gen521 6. Lights 7. Exhaust duct

Table 1: List of measuring devices

Position	Code		Accuracy	Description
Temperature measurements				
Fuel cell generator				
Left stack thermocouples				
1	T3	Below left stack	±2.2°C	K type Inconel sheathed
2	T5	Left stack	±2.2°C	K type Ceramic sheathed
3	T7	Above left stack	±2.2°C	K type Inconel sheathed
4	T8	Above left center stack	±2.2°C	K type Inconel sheathed
Right stack thermocouples				
5	T1	Right stack air plenum (manifold end)	±2.2°C	K type Inconel sheathed
6	T2	Right stack air plenum (cell end)	±2.2°C	K type Inconel sheathed
7	T4	Below right center stack	±2.2°C	K type Inconel sheathed
8	T6	Right stack CM1	±2.2°C	K type Ceramic sheathed
9	T9	Above right center stack	±2.2°C	K type Inconel sheathed
10	T10	Above right stack	±2.2°C	K type Inconel sheathed
Other equipment thermocouples				
11	T15	Exhaust fan1 - inlet	±2.2°C	K type Ceramic sheathed
12	T12	Exhaust fan2 - inlet	±2.2°C	K type Ceramic sheathed
13	T13	Heat exchanger out (cell end)	±2.2°C	K type Inconel sheathed
14	T14	Between off gas and burner (cell end)	±2.2°C	K type Ceramic sheathed
15	T16	Exhaust duct	±2.2°C	K type Ceramic sheathed
16	T17	Water coil inlet	±2.2°C	K type Ceramic sheathed
17	T18	Water coil outlet	±2.2°C	K type Ceramic sheathed
18	T19	Batteries	±2.2°C	K type Heat shrink sheathed
19	T20	Power conditioning compartment	±2.2°C	K type Heat shrink sheathed
Electrolyzer				
20		Oxygen gas in cell	±0.5°C	Pt 100 thermal resistance
21		Hydrogen gas in cell	±0.5°C	Pt 100 thermal resistance
22		Electrolyte	±0.5°C	Pt 100 thermal resistance
Pressure measurements				
Fuel cell generator				
23		Hydrogen fuel cells inlet pressure	±0.8 mbar	Piezoresistive sensor
24		Air pressure in one stack	±0.05 mbar	Pressure gauge
Electrolyzer				
25		Hydrogen cell pressure	±0.12 bar	Extensometric pressure transducer
26		Oxygen cell pressure	±0.12 bar	Extensometric pressure transducer
Dryer				
27		Dryer pressure	±0.1 bar	Pressure gauge
Voltages				
Fuel cell generator				
from 28 to 51		24 measurement points for 24 fuel cell manifolds (6 cells/manifold)	±0.01Volt	
Mass flow rate measurements				
Fuel cell generator				
54	MFC1	Hydrogen for anode	±0.01 l/s	Mass flow controller
55	MFC2	Hydrogen for burner	±0.01 l/s	Mass flow controller
56	BL1	Air blower	relation from rpm	
Electrolyzer				
58		Hydrogen volume flow rate	±0.7 normal l/s	From unit calibration curve
59		Oxygen volume flow rate	±0.7 normal l/s	From unit calibration curve

3. The Acumentrics Gen521 SOFC generator

The Acumentrics generator (Gen521) consists of two SOFC stacks, a set of components belonging to the BoP (blowers, control valves and heat exchangers) and a PCS for treating the DC electrical power. The unit can produce 2.5kW of rated electrical power, it is 86 x 145 x

127 cm in size and weighs 794kg (batteries included). The generator has 144 tubular anode-supported solid oxide cells divided into two stacks. Each stack is assembled in 2 separate blocks. Each block is made of 6 overlapping rows, with 6 cells placed in series in each row (Figure 2). Each cell is 1.5cm in diameter and 33cm long, with an anode about 0.15cm thick, an active surface of 133cm^2 and a horizontal position. Air flows around the outside of the cells (cathode side) and hydrogen through the inside (anode side) using an internal distributor tube. The anode is a cermet of nickel oxide and yttria-stabilized zirconia to support the weight of the cell, the electrolyte is pure yttrium-oxide-stabilized ZrO_2 (YSZ) and the cathode is lanthanum-strontium manganite (Sr-dopped $LaMnO_3$). The interconnections are in lanthanum chromite ($LaCrO_3$). The cathode current collector is made of silver. The characteristics of the single cells are therefore similar, in terms of the materials and design, to those described in [30].

Each stack works with a vertical thermal gradient during its operation and each single row of cells operates at a different temperature, with a negligible horizontal thermal gradient. Figure 2 shows the process and instrumentation diagram, showing the BoP components. Hydrogen is fed into the unit and divided into two streams. One stream flows through a normally-closed solenoid valve SV1 and a mass flow controller MFC1 to feed the fuel cells. Along this path, the hydrogen is pre-heated in a heat exchanger with the fluid entering the cathode side stack. The second stream of hydrogen flows through a normally-closed solenoid valve SV2 and a mass flow controller MFC2, then it is sent to the burner, where the combustion of the hydrogen from the second stream, the excess hydrogen recirculating from the stack and the outside air takes place. The blowers BL1 and BL2 deliver outside air to the SOFC generator to reach the flow rate needed for the electrochemical reaction and combustion.

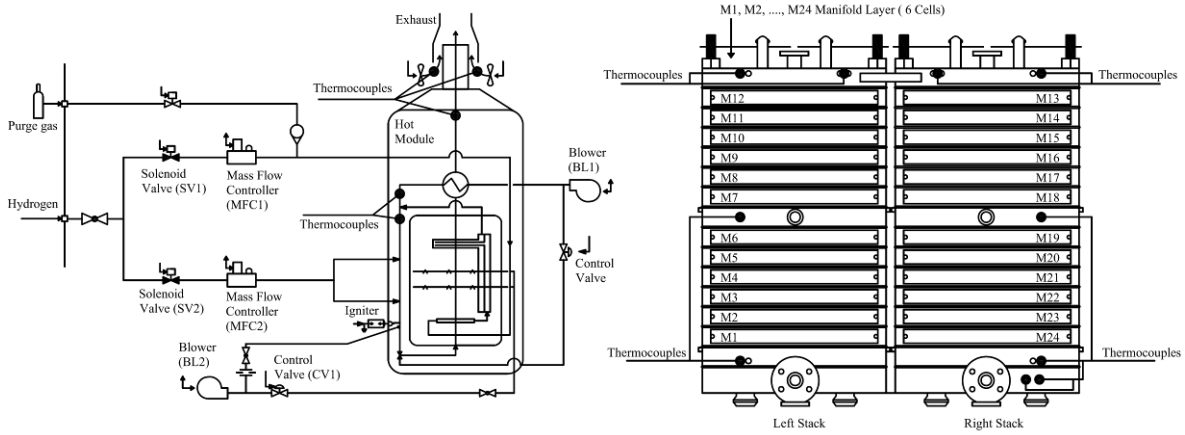

Figure 2. Process & instrumentation diagram and map of measuring devices

As for the PCS, in a fuel cell generator this is typically made as explained in [31]. In the particular case of the Gen521, the PCS consists of a first stage to set the stack output voltage to 48V DC. The power obtained from this DC/DC converter is stored in 4 batteries and then sent to the inverter. Priority is given to the batteries because they serve as a buffer useful for powering the BoP components during unit start-ups, or for restarting after a malfunction. Finally, the power converted by the inverter feeds a set of 5 lights (400W rated), each of which represents an electrical load; this configuration enables the electrical loads to be set at various levels (400W, 800W, 1200W, 1600W, 1800W). The load can also be varied continuously, allowing the system to work at intermediate electrical loads by means of a variac.

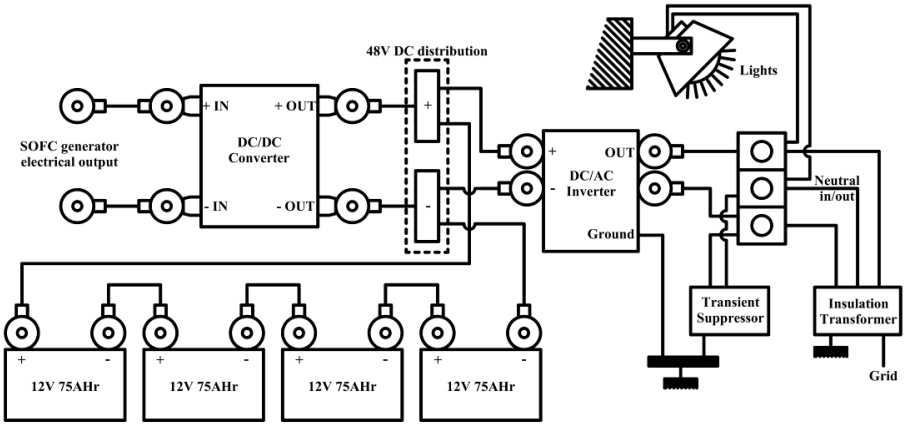

Figure 3. Block diagram of the SOFC generator PCS

4. Gen521 generator operation

On start-up, the generator stacks are brought from ambient temperature beyond a temperature set-point (typically 680°C) using the hydrogen/air mixture in the burner. When this threshold has been exceeded, the electric circuit between the stacks and the user is closed, placing the load and the batteries in contact with the generator. During this first phase the batteries are charged, taking priority over the electrical load. Within a few hours the temperature of the stack becomes stable generally within a range of 760°C to 850°C, depending on the operating conditions, with an internal vertical thermal gradient that in normal operating conditions is approximately 40°C. When the balance is reached, the burner is used exclusively to control the temperature of the stacks. The valve CV1 simultaneously delivers outside air for the cooling of the stacks. All controls implemented inside the system are handled by means of proportional-integral loops that take effect with default parameters established by Acumentrics Corp. The generator is monitored and controlled by an internal programmable logic controller connected to a software implemented on a remote PC.

5. SOFC generator testing strategy

The experiments were designed to establish the unit's performance in terms of SV and DC electrical power in different operating conditions. In particular, only the steady state working conditions were considered, so the tests consisted in changing some adjustable parameters and the electrical loads to 400W, 800W, 1200W, 1000W and 1400W. The experimental data were obtained by combining the results recorded in these different operating conditions. The results were typically arrays of time-dependent values. This very large set of collected data was filtered using four criteria:

1. stack temperatures: each temperature value acquired had to be no more than 2.5°C higher or lower than the mean temperature measured for the previous 600 s;
2. the voltages measured for the 24 stacks: each voltage value acquired had to be no more than 0.01V higher or lower than the mean voltage measured for the previous 600 s;
3. battery voltage: each battery voltage value acquired had to be no more than 0.075V higher or lower than the mean voltage measured for the previous 600 s;
4. residence time of the value measured: all measured values had to satisfy the above conditions for at least 30 s.

The data acquired were thus reduced in number and were representative of genuinely stable operating conditions. The experimental data gave rise to numerous clusters, as shown in Figure 4, so they were difficult to interpret and group into common working conditions illustrating the unit's operation. In fact observing the dependence of DC electrical power and SV on the current, in Figure 4 might seem that there are three operating conditions. Actually

the operating stable conditions are more than three. The scatter plots in Table 3 show numerous clusters and so several functioning points. Therefore one has to take into account not only the current but also other equally important parameters studying the dependence between such parameters, the DC electrical power and SV. A multivariate analysis allows the study of the unit operation in this way. By adopting this method for data analysis it is possible define relations on the dependence between the parameters selected as significant and the performance (DC electrical power and SV). So after identifying the system's input parameters and output variables, any stable system operating conditions are presented as a vector of the data, each available vector differing from the others. Regression of the experimental vectors can be done using the response surfaces method. This method can be applied to different types of analysis, the most straightforward (and consequently best documented) being multivariate polynomial interpolation. This method leads to the formulation of polynomials, however, and consequently often gives rise to surfaces that are not monotonous in the domain of interest.

Therefore it was chosen to regress the experimental data using the multilinear (or linearizable) regression method, also based on the results of a PCA [32]. The identification of a multilinear (or linearizable) response surface based on considerations from the PCA led to a simplified relationship between several independent parameters (inputs) and the dependent variable (output) of interest. In fact, PCA enables a subset of parameters to be selected to formulate more than one regression equation. These relations can be determined by means of a subsequent multivariate regression on some selected input parameters.

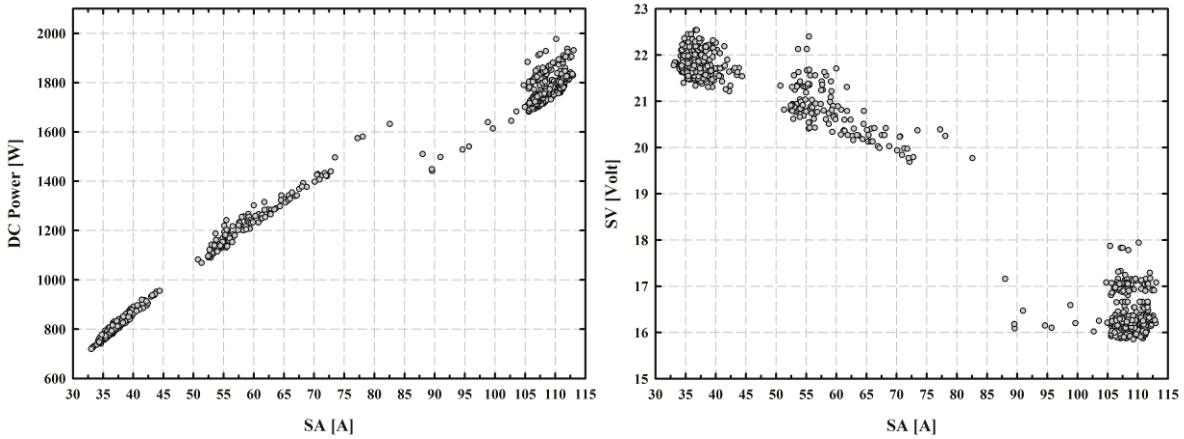

Figure 4. Experimental data collected for DC electrical power and SV in a steady state for different currents generated by the stacks

6. Pattern recognition

As emerges from the experimental data collected in Figure 4, there was a higher density of acquisitions in certain current ranges because the tests were conducted at different electrical loads. Figure 4 also shows a discontinuity in the DC electrical stack power (before the DC/DC converter) at around 85 A.

This discontinuity highlights the different operating conditions imposed on the machine at the higher currents. Given this discontinuous trend of the DC stack power (DC power) and SV, it became necessary to divide the operating domain between the higher currents (from 88.00 A to 112.8 A) and the lower currents (from 33.02 A to 82.57 A). These two zones into which the study was divided had the characteristics outlined in Table 2. Looking at the data in Table 2, the largest differences between the two datasets for the operating zones 1 and 2 clearly coincide with the global thermal gradient of the stacks (DT), the mean working temperature

of the stacks (TM) and the utilization factor (FU). So our proposed characterization will therefore be divided into two parts depending on the stack current (SA) range.

Table 2: Description of the parameters and variables under investigation in zones 1 and 2

Parameters	Units	I/O	Meaning	Zone 1		Zone 2	
				Minimum	Maximum	Minimum	Maximum
AirF	m^3/s	Input	Cathode air flow rate	0.00945	0.03183	0.01297	0.01550
HyF	m^3/s	Input	Anode hydrogen flow rate	0.00043	0.00059	0.00043	0.00047
HyP	Pa	Input	Anode hydrogen pressure	101328	101807	101328	101807
RAirHy	--	Input	Ratio between cathode and anode flow rates	21.11	55.57	28.96	33.86
SA	A	Input	Current form the two stacks of the generator	33.02	82.57	88.00	112.80
TM	°C	Input	Mean temperature in the stacks	767.20	811.15	739.30	758.70
DT	°C	Input	Difference between maximum and minimum temperatures in the stacks	37.20	42.3	88.00	119.30
FU	%	Input	Utilization factor	19.45	37.49	46.90	72.77
SV	V	Output	Stacks voltage	19.69	22.54	15.85	17.94

7. Analysis of the experimental data

The table 3 shows the scatter plot and correlation matrix for the whole data set (zones 1 and 2). Significant correlation coefficients are in bold and were obtained considering the values outside the range ±0.500. Table 3 shows the plots of the coupled variables. Several clusters can be seen, which make it difficult to generalize the machine's operation. Table 3 shows some of the correlations in the machine's operation; some of them depend on the control system, which correlates certain variables that are themselves not correlated.

Table 3: Scatter plot and correlation matrix on the experimental data collected

	AirF	HyF	HyP	RAirHy	SA	TM	DT	FU	DC Power	SV
AirF										
HyF	**0.969**									
HyP	-0.165	-0.147								
RAirHy	**0.989**	**0.923**	-0.164							
SA	0.082	-0.093	0.048	0.213						
TM	**0.559**	**0.700**	-0.138	0.437	**-0.749**					
DT	-0.146	-0.324	0.083	-0.009	**0.941**	**-0.899**				
FU	-0.062	-0.241	0.068	0.073	**0.982**	**-0.834**	**0.967**			
DC Power	0.180	0.008	0.032	0.306	**0.992**	**-0.676**	**0.967**	**0.958**		
SV	0.020	0.194	-0.061	-0.111	**-0.983**	**0.807**	**-0.957**	**-0.986**	**-0.954**	

In other cases, the parameters are correlated as a consequence of physical phenomena that influence each other. In other cases again, certain parameters are estimated starting from other parameters. Note that the flow of hydrogen to the anode (HyF) correlates with the air flow to the cathode (AirF), and HyF and AirF correlate with TM. In particular TM correlates more closely with HyF than with AirF. In addition TM is related to the current produced. FU naturally correlates with SA and with the parameters connected to the machine's temperature conditions TM and DT (DT is calculated as the difference between the maximum and minimum temperatures acquired, while TM is the arithmetical mean between the same two values). Finally, there are some less evident correlations: for instance, DT correlates with SA (and obviously with TM). DC Power and SV are considered machine output parameters. They are practically correlated with all the variables. In particular they are indirectly correlated with HyF and AirF and consequently also RAirHy through TM. The hydrogen pressure at the

anode inlet (HyP) does not correlate with any variable and this may be justified by the fact that, as shown in Table 2, HyP has a very limited range of variation around atmospheric pressure. Now it is possible to apply to the data the procedure shown in Figure5. As a first step the PCA on the study zones is performed, then a multi-linear regression and eventually a full factorial design on the developed equation to identify the most important operational parameters.

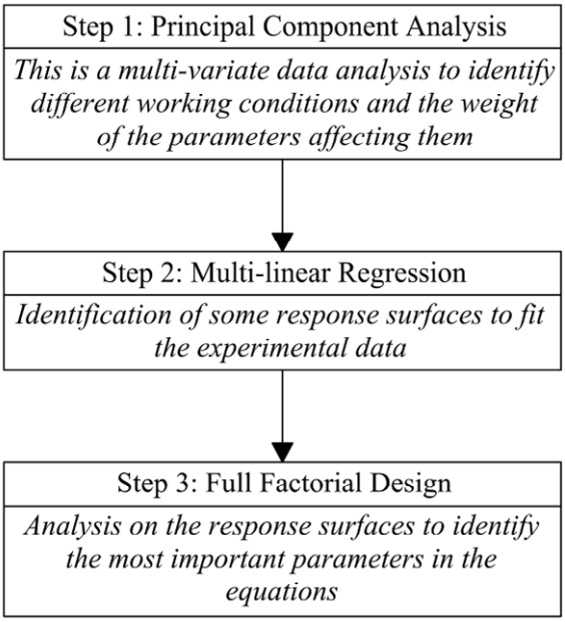

Figure 5. Procedure for the data analysis

The data had to be scaled first, however, because the units of measure of each parameter and variable differed. Conducting the analysis without completing this important preliminary step would produce erroneous results because they would be influenced by the very different order of magnitude of the numerical values. For instance, it would be wrong to treat HyP and DT in the same analysis because their numerical values have different orders of magnitude and different variances. Data scaling is therefore a step that enables the effects of different units of measure and variances on the PCA to be minimized. This scaling can be done in various ways. For the present problem, it was opted for a natural-logarithmic scaling of the data due to the large differences in the orders of magnitude between the numerical values and between their variances [33]. Then the PCA was conducted on the scaled data. PCA is mathematically defined as an orthogonal linear combination that transforms the data to a new coordinate system having the PCs as axes. PCA is a multivariate analysis of data method performed on a dataset for the purpose of identifying a limited number of parameters that account for most of the variance of the data. The method is therefore used to establish which parameters determine similarities between the data. In PCA the original set of (correlated or uncorrelated) parameters is converted into a new set comprising an equal number of independent uncorrelated principal components (PCs), which are linear combinations of the original parameters. Along the first coordinate (PC1) the greatest variance of data is present, then the second coordinate (PC2) adds another part of variance of data and so on for all PCs."Along the first coordinate (PC1) is present the greatest variance of data, adding the second coordinate (PC2) it is explained another part of variance of data and so on for all PCs. At the end of the analysis, it is also obtained a sequential list of linear combinations that best explain the variance of the data and from these combinations it is possible to identify the parameters that affect the variance the most. From the viewpoint of the similarity of data instead of the

variance, projecting the data onto a space that depends on the linear combination of the parameters enables us to identify any clusters, which represent similar operating conditions. By applying PCA to the data, the loadings of the parameters on the various PCs were obtained.

Clearly, other methods of clustering or classification could be adopted, such as the Gastofan-Kessel clustering [34] or self organization mapping [35] to obtain more precise divisions. Table 4 shows the loadings of the PCs for the data in zones 1 and 2.

Table 4: Loadings of the parameters measured on the rotated factors

	PC1	PC2	PC3	PC4	PC5	PC6	PC7	PC8
Zone 1								
AirF	0.021	0.001	0.012	0.004	0.116	0.007	0.993	0.007
HyF	0.000	0.000	0.000	0.000	0.003	0.001	0.006	-1.000
HyP	-0.001	0.000	-0.002	0.000	0.056	-0.998	0.001	0.000
RAirHy	0.821	0.103	0.503	0.243	-0.046	-0.004	-0.019	0.000
SA	0.529	-0.100	-0.527	-0.657	-0.018	0.000	0.000	0.000
TM	0.046	-0.036	0.018	0.001	0.990	0.055	-0.117	0.002
DT	-0.013	0.986	-0.160	-0.034	0.039	0.003	-0.003	0.000
FU	0.207	-0.081	-0.665	0.713	-0.001	0.001	0.001	0.000
% of variance explained	79.8%	15.8%	3.2%	1.2%	0.0%	0.0%	0.0%	0.0%
Eigenvalue	0.145	0.029	0.006	0.002	0.000	0.000	0.000	0.000
Zone 2								
AirF	-0.006	0.004	-0.013	-0.003	0.001	0.068	0.997	-0.032
HyF	0.000	0.000	0.000	0.000	0.000	0.002	0.031	1.000
HyP	-0.001	-0.001	0.000	0.001	0.023	0.997	-0.068	0.000
RAirHy	-0.235	0.329	-0.910	-0.096	0.005	0.000	-0.015	0.000
SA	-0.037	0.014	0.119	-0.992	0.001	0.001	-0.001	0.000
TM	-0.074	0.010	0.028	0.007	0.997	-0.023	0.000	0.000
DT	0.942	-0.138	-0.285	-0.071	0.080	-0.001	0.002	0.000
FU	0.223	0.934	0.276	0.038	-0.001	0.002	0.001	0.000
% of variance explained	47.4%	25.2%	15.9%	11.4%	0.0%	0.0%	0.0%	0.0%
Eigenvalue	0.003	0.002	0.001	0.001	0.000	0.000	0.000	0.000

In common practice only the loadings with an absolute value higher than 50% are considered. For both the zones, the analysis suggested that the first 4 PCs explain 100% of the variance of the data, but the most important PCs for zone 1 were PC1 and PC2 (95.6% of the variance), while PC1, PC2, PC3, PC4 were all important for zone 2.

Figure 6 shows the experimental data for zone 1 as a function of PC1 and PC2, where it can be seen the previously described effects. Intuitively, there are three clusters identifiable on the strength of PC1 e PC2.

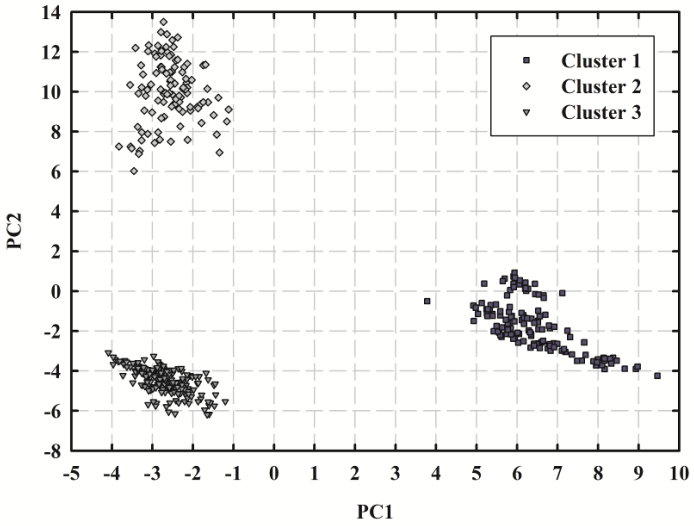

Figure 6. Experimental data on the PC1-PC2 hyperspace

From the data for zone 1, it were obtained the three clusters shown in Figure 6 on the plane PC1-PC2. From the data for zone 2, it were obtained the two clusters shown in Figure 7. In this latter case, it was need to check the distribution of the data in all the first four PCs due to the variance is more evenly divided between them.

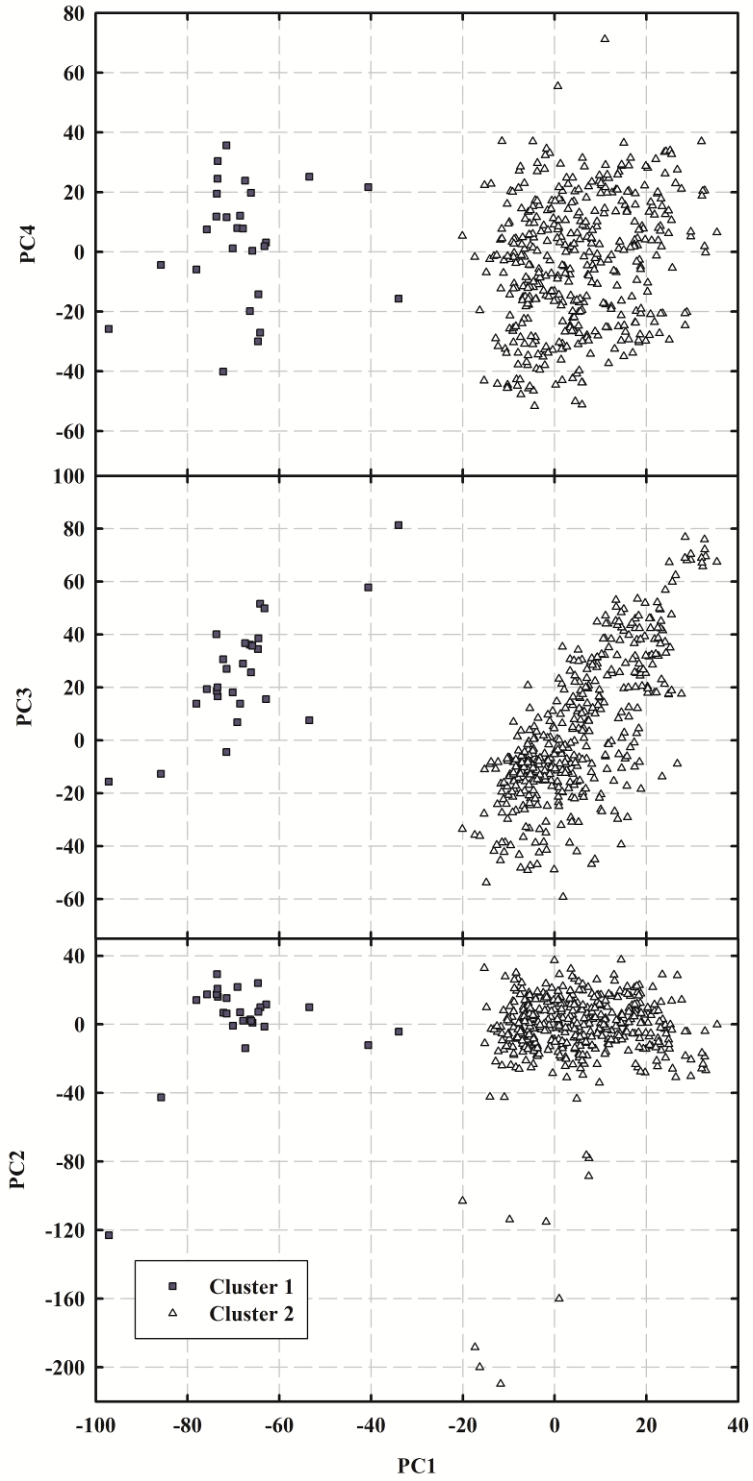

Figure 7. Experimental data on the hyperspaces PC1-PC2, PC1-PC3, PC1-PC4

The identification of different clusters leads to the determination of different operating conditions. Thus by separately analyzing the data belonging to each cluster and the principal differences between the clusters, it can be identified which parameters influence the machine's performance.

To identify these parameters the most often-used method consists in performing a stepwise regression using the PCs [36, 37]. Table 5 shows the steps involved in the stepwise regression and the corresponding results.

Table 5: Stepwise regression using the principal components

SV				Parameters driving the variance
Zone 1	PC1			RAirHy; SA
Adjusted R^2	0.605			
Estimated regression coefficient	0.0258271			
Constant	22.4054			
Zone 2	PC1	PC1+PC4	PC1+PC4+PC3	DT; RAirHy; SA
Adjusted R^2	0.007	0.009	0.018	
Estimated regression coefficient	-0.00641972	-0.00637817	-0.0104894	
Constant	16.1282	16.2882	16.5763	
DC Power				
Zone 1	PC1	PC1+PC7		RAirHy; SA; AirF
Adjusted R^2	0.935	0.936		
Estimated regression coefficient	11.9015	13.5255		
Constant	513.6	337.029		
Zone 2	PC4	PC4+PC8		SA; HyF
Adjusted R^2	0.543	0.543		
Estimated regression coefficient	69.9233	74.0108		
Constant	0	0		

Adjusted $R^2=1-\{[(n-1)(1-R^2)]/(n-p)\}$ where n is the number of data and p is the number of parameters in the model. Adjusted R^2 gives a modified version of the coefficient of determination R^2 which adjusts for the number of parameters in the model.

The parameters that determine the similarity of the data are for SV, RAirHy and SA in zone 1, and DT as well in zone 2. Such results show that the main difference in the data collected for the operation between zones 1 and 2 consists in the thermal gradient inside the stacks.
For DC Power in zone 1 the similarity of the data is given by similar values for RAirHy, SA and AirF. SA remains for zone 2, while RAirF and AirF no longer contribute to the variance of the data. It can be concluded that DC Power depends primarily on SA in zone 2 and secondarily on HyF, since the introduction of the parameter HyF does not appear to be particularly important for the regression. The low value of the adjusted R-square in zone 2 of SV demonstrates that the correlation between SV and its parameters is not linear. DC Power in zone 2 is also non-linear in relation to its parameters, but less than SV. In zone 1, on the other hand, the adjusted R-square values suggest that both SV and DC Power have a linear trend.
Finally, it should be noted that Table 5 shows the parameters that influence the variance of the data. So the PCA was used to measure the significance of the selected parameters on the differences between clusters of data. To formulate a correlation based exclusively on these parameters would be an oversimplification because using the parameters deduced by PCA alone would not enable a sufficiently accurate description of the variation in SV and DC Power within a given cluster. To describe the passage between several steady states, other parameters in addition to those selected, were need to introduce. On the other hand, if a rough estimate of the machine's operation were sufficient, the selection of the identified parameters could be sufficient.

8. Results

The above-described analysis enabled us to select a subset of parameters for modeling the unit's operating conditions. Figure 4 shows a close correlation between SA and DC Power from which the correlation between SA and SV (the unit's polarization curve) could also be derived. As shown in Figure 4, this correlation cannot be derived by direct regression of the data on SV because these data form several clusters. Based on the previous PCA it could be developed a simplified equation in order to correlate SV and DC Power, involving a few significant parameters, or more complex models could be developed, considering all the parameters, by means of a multivariate regression. Finally, two models needed to be developed, one for each zone investigated. Thus, the correlations adopted for the regressions were:

$$SV = a_{SV,0} + \beta_{SV,1}\, AirF + \beta_{SV,2}\, HyF + \beta_{SV,3}\, HyP + \beta_{SV,4}\, RAirHy + \beta_{SV,5}\, (SA \text{ or } Log(SA)) + \beta_{SV,6}\, TM + \beta_{SV,7}\, DT + \beta_{SV,8}\, FU$$

$$DC\ Power = a_{Pow,0} + \beta_{Pow,1}\, AirF + \beta_{Pow,2}\, HyF + \beta_{Pow,3}\, HyP + \beta_{Pow,4}\, RAirHy + \beta_{Pow,5}\, (SA \text{ or } Log(SA)) + \beta_{Pow,6}\, TM + \beta_{Pow,7}\, DT + \beta_{Pow,8}\, FU$$

where Log is the natural logarithm. Table 6 shows the coefficients derived from the various regressions by means of increasingly simple models for each operating zone, for both SV and DC Power. In addition to the adjusted R-square, table 6 also shows other equally important parameters to confirm the validity of the regression.

Table 6: Coefficients of the models

	$a_{SV,0}$	$\beta_{SV,1}$	$\beta_{SV,2}$	$\beta_{SV,3}$	$\beta_{SV,4}$	$\beta_{SV,5}$ for SA	$\beta_{SV,5}$ for Log(SA)	$\beta_{SV,6}$	$\beta_{SV,7}$	$\beta_{SV,8}$	R^2_{adj}	Max Res.	Min Res.	Std Dev res.	Mean res.	Curv.95% Conf. Reg.
SV zone 1																
1	11.81300	-336.752	-190.904	9.602E-05	0.220732	--	-0.71307	0.00246678	-2.73473E-03	-0.0293085	1.000	1.25	-0.70	0.291	5.8E-14	0.73
2	8.13357	-325.501	498.645	1.047E-04	0.210996	-0.0200075	--	0.00324554	-2.06736E-03	-0.0232869	0.694	1.25	-0.69	0.289	7.2E-14	--
3	18.32110	-305.997	-283.428	--	0.199811	-0.0199294	--	0.00425978	-1.17993E-03	-0.0228407	0.694	1.25	-0.69	0.289	1.7E-13	--
4	21.14940	-318.793	-900.047	--	0.210414	--	-0.712603	0.00340237	-1.91832E-03	-0.0288458	1.000	1.24	-0.68	0.291	1.4E-13	0.72
5	57.97540	--	--	--	0.037737	--	-1.08404	-0.04037630	-2.39862E-02	-0.0309108	1.000	1.27	-0.74	0.298	7.5E-14	0.69
6	61.01390	--	--	--	0.042950	--	-1.49599	-0.04338920	-2.56236E-02	--	1.000	1.23	-0.74	0.302	1.5E-13	0.67
7	29.62660	--	--	--	0.004590	--	-2.20535	--	-2.25639E-04	--	1.000	1.39	-0.70	0.311	5.1E-15	0.65
8	23.74580	--	--	--	0.002195	-0.0388318	--	--	-1.206E-04	-0.0246614	0.669	1.38	-0.63	0.300	8.3E-15	--
9	23.39010	--	--	--	0.004089	-0.0465218	--	--	--	--	0.663	1.36	-0.62	0.303	1.2E-14	--
10	29.59930	--	--	--	0.004510	--	-2.200100	--	--	--	1.000	1.39	-0.70	0.311	3.0E-15	0.62
zone 2																
1	-36.1716	-1259.1	48582.8	-8.602E-05	0.652632	--	0.266212	0.0428924	2.82523E-02	0.00348682	0.999	1.59	-0.58	0.393	-1.8E-14	0.73
2	-35.0962	-1252.99	48373.4	-8.604E-05	0.649883	0.00270312	--	0.0428627	2.82373E-02	0.0034719	0.084	1.59	-0.58	0.393	-1.4E-14	--
3	-42.2718	-1165.23	45127.3	--	0.610807	0.00294537	--	0.0427279	2.80039E-02	0.00339615	0.084	1.58	-0.58	0.393	-5.4E-14	--
4	-43.4563	-1172.18	45363.9	--	0.613938	--	0.292343	0.042761	2.80207E-02	0.00341076	0.999	1.58	-0.58	0.393	-3.5E-14	0.72
5	-23.5991	200.413	789.577	--	--	--	0.284133	0.0428826	2.81078E-02	0.0036659	0.999	1.58	-0.56	0.394	2.1E-14	0.70
6	-23.4468	202.219	352.929	--	--	--	0.304934	0.0430795	2.83368E-02	--	0.999	1.59	-0.56	0.394	1.4E-14	0.69
7	11.6866	184.838	497.253	--	--	--	0.291907	--	3.13688E-03	--	0.999	1.59	-0.63	0.396	2.8E-14	0.67
8	12.7324	184.808	484.647	--	--	0.00302454	--	--	3.13880E-03	--	0.073	1.59	-0.63	0.396	1.1E-14	--
9	13.2315	--	--	--	0.081056	0.00548060	--	--	-1.10149E-03	--	0.059	1.59	-0.68	0.399	-1.5E-16	--
10	11.2887	--	--	--	0.0810833	--	0.541629	--	-1.11683E-03	--	0.999	1.59	-0.68	0.399	1.6E-15	0.65
DC Power zone 1	$a_{Pow,0}$	$\beta_{Pow,1}$	$\beta_{Pow,2}$	$\beta_{Pow,03}$	$\beta_{Pow,4}$	$\beta_{Pow,5}$ for SA	$\beta_{Pow,5}$ for Log(SA)	$\beta_{Pow,6}$	$\beta_{Pow,7}$	$\beta_{Pow,8}$	R^2_{adj}	Max Res.	Min Res.	Std Dev res.	Mean res.	Curv.95% Conf. Reg.
1	-4074.78	-5038.52	-17626.0	9.491E-03	2.36355	--	924.802	0.691061	0.510723	0.960723	1.000	88.13	-37.71	16.511	-4.6E-12	0.73
2	-173.773	13761.3	-84450.9	1.188E-03	9.85715	19.8712	--	0.149788	-0.17297	-1.72452	0.994	68.13	-43.37	14.581	-2.6E-12	--
3	-58.1905	-13540.0	-93323.8	--	9.73026	19.8721	--	0.161295	-0.162902	-1.71945	0.994	68.05	-43.39	14.582	-2.1E-12	--
4	-3151.99	-3263.5	-87715.8	--	1.34378	--	924.848	0.783533	0.591415	1.00645	1.000	86.88	-38.25	16.537	-6.0E-12	0.72
5	-2559.11	--	--	--	-0.443755	--	918.421	0.0363714	0.193264	0.972946	1.000	88.05	-39.04	16.571	-3.1E-12	0.69
6	-2654.75	--	--	--	-0.607853	--	931.388	0.131203	0.244803	--	1.000	91.60	-40.42	16.639	-7.7E-12	0.67
7	-2559.84	--	--	--	-0.491857	--	933.533	--	0.168003	--	1.000	91.75	-39.89	16.641	-3.3E-12	0.65
8	138.571	--	--	--	0.663816	18.8688	--	--	-0.09583	-1.8154	0.994	75.30	-42.71	15.208	1.9E-12	--
9	3.0009	-13410.30	--	--	9.510860	19.2923	--	--	--	--	0.994	68.87	-47.52	14.949	2.6E-12	--
10	-2587.06	-2685.93	--	--	1.309	--	938.993	--	--	--	1.000	92.68	-39.13	16.676	1.5E-12	0.65
zone 2																
1	-12912.3	-188745.0	6968170	-7.919E-03	74.2735	--	1710.24	4.89874	3.18359	0.410075	0.999	175.57	-64.04	42.733	-4.5E-12	0.73
2	5700.26	-144142.0	5503630	-9.681E-03		16.6415	--	4.6973	3.08297	0.371373	0.596	174.71	-63.52	42.637	-4.2E-12	--
3	-6507.71	-134267.0	5138360	--	94.3801	16.6687	--	4.68214	3.0567	0.362848	0.595	174.27	-64.09	42.648	-6.8E-12	--
4	-13583.0	-180744.0	6671820	--	69.8763	--	1712.65	4.88663	3.16227	0.403072	0.999	175.21	-64.50	42.740	5.4E-13	0.72
5	-10645.6	22300.1	78084.9	--	90.8177	--	1711.43	4.90463	3.17516	0.440814	0.999	175.24	-61.58	42.759	6.4E-13	0.70
6	-10627.3	22517.3	25579.2	--	--	--	1713.93	4.92831	3.2027	--	0.999	176.14	-60.95	42.774	7.6E-13	0.69
7	-6608.0	20528.9	42089.9	--	--	--	1712.44	--	0.319817	--	0.999	176.65	-68.87	43.031	8.9E-13	0.67
8	-385.644	20248.6	33612.4	--	--	16.6767	--	--	0.331806	--	0.590	175.56	-68.88	42.907	2.0E-13	--
9	-348.372	--	703575	--	--	16.6155	--	--	--	--	0.565	176.84	-49.62	44.160	5.7E-14	--
10	-6545.72	--	727045	--	--	--	1704.84	--		--	0.999	177.95	-47.62	44.317	3.9E-12	0.62

Completely linear and linearizable models were derived, but curvature tests can be performed in the latter, not in the former. The difference between the two classes of equations consists in the introduction of the natural logarithm of SA in the case of the non-linear models. Introducing this non-linear parameter enables us to obtain the coefficient of determination much higher and to concentrate the study on the curvature tests. The curvature was assessed on a confidence interval (95%) centered on the least-squares parameter estimates. The curvature in Table 6 is a scaled measure of the radius of curvature of the parameter space. Generally speaking, the non-linear expressions with a higher curvature were those most closely following the experimental data in zone 2 of SV and DC Power. The models on which the subsequent considerations were based are those identified with the numeral 1 in Table 6 and are listed below.

For SV in zone 1:

SV= 11.8130 -336.752AirF -190.904HyF +9.602E-05HyP +0.220732RAirHy -0.71307Log(SA) +0.00246678TM -2.73473E-03DT -0.0293085FU *(1)*

For SV in zone 2:

SV= -36.1716 -1259.1AirF +48582.8HyF -8.602E-05HyP +0.652632RAirHy +0.266212Log(SA) +0.0428924TM +2.82523E-02DT +0.00348682FU *(2)*

For DC Power in zone 1:

DC Power= -4074.78 -5038.52AirF -17626.0HyF +9.491E-03HyP +2.36355RAirHy +924.802Log(SA) +0.691061TM +0.510723DT +0.960723FU *(3)*

For DC Power in zone 2:

DC Power= -12912.3 -188745.0AirF +6968170HyF -7.919E-03HyP +74.2735RAirHy +1710.24Log(SA) +4.89874TM +3.18359DT +0.410075FU *(4)*

Figure 8 shows the regression of the experimental data with eqns. (1-4) for SV and DC Power in zones 1 and 2. These models were selected because:
1) they have a greater curvature. For SV it is important to take the parameters other than SA into account as well because the operating domain of SV is very limited. This obliges the accuracy of the correlations to be lower than the first decimal digit. In fact, a model based entirely on SA could be developed, but it would not be useful for mapping the experimental points. The parameterization of the data entails the need to distinguish differences at least in the first decimal digit. For DC Power the curvature test shows that, if it wishes to remain with curvatures higher than 0.7, there is no advantage in selecting a relationship characterized by a number of parameters slightly lower than those involved in (3) and (4). In fact, in zone 2, DC Power acquires a curvature for high currents. To follow this behavior it is needed to introduce non-linear model in the same way as for SV;
2) being composed of all the parameters investigated, the proposed models are suitable for estimating the influence of every single factor on the output of interest (SV or DC Power) by means of a two-level full factorial design (FFD) [38].
Figure 8 shows the correctness of the fit for the experimental data with the eqns. (1-4). The analysis of the residuals is shown in Figure 9. In zone 1, the equations (1) and (3) regress the experimental data with a satisfactory accuracy. In zone 2, it can be seen that the equation (4) produces accurate results, while equation (3) reveals a strong non-linearity of the data. This suggests that, in order to improve the model (3), it would be necessary to formulate an alternative non-linear correlation. Although the model (3) is the only one proving critical among those developed, the coefficient of determination and the curvature are still sufficiently high, so even equation (3) was considered valid, albeit with a lower accuracy than those obtained in the regressions of the corresponding experimental data using equations (1), (2) and (4).

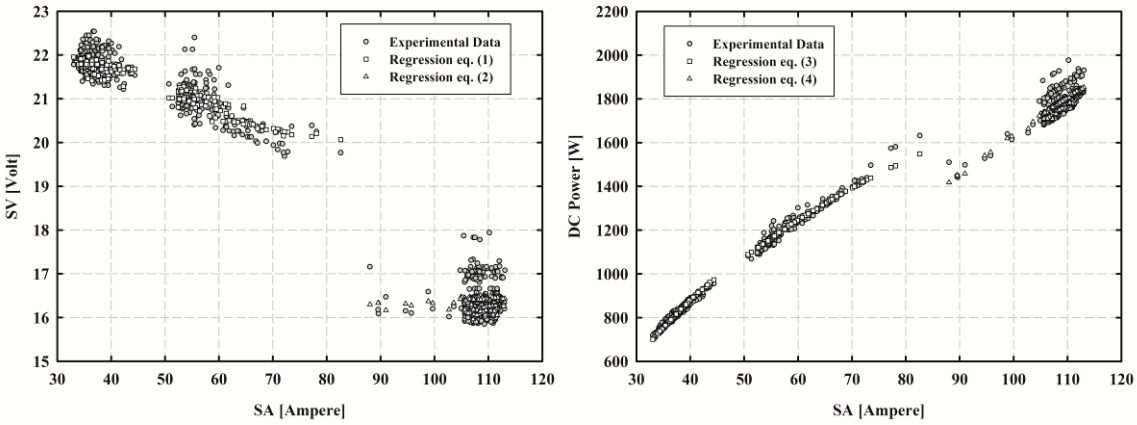

Figure 8. Regression of the experimental data with the models selected

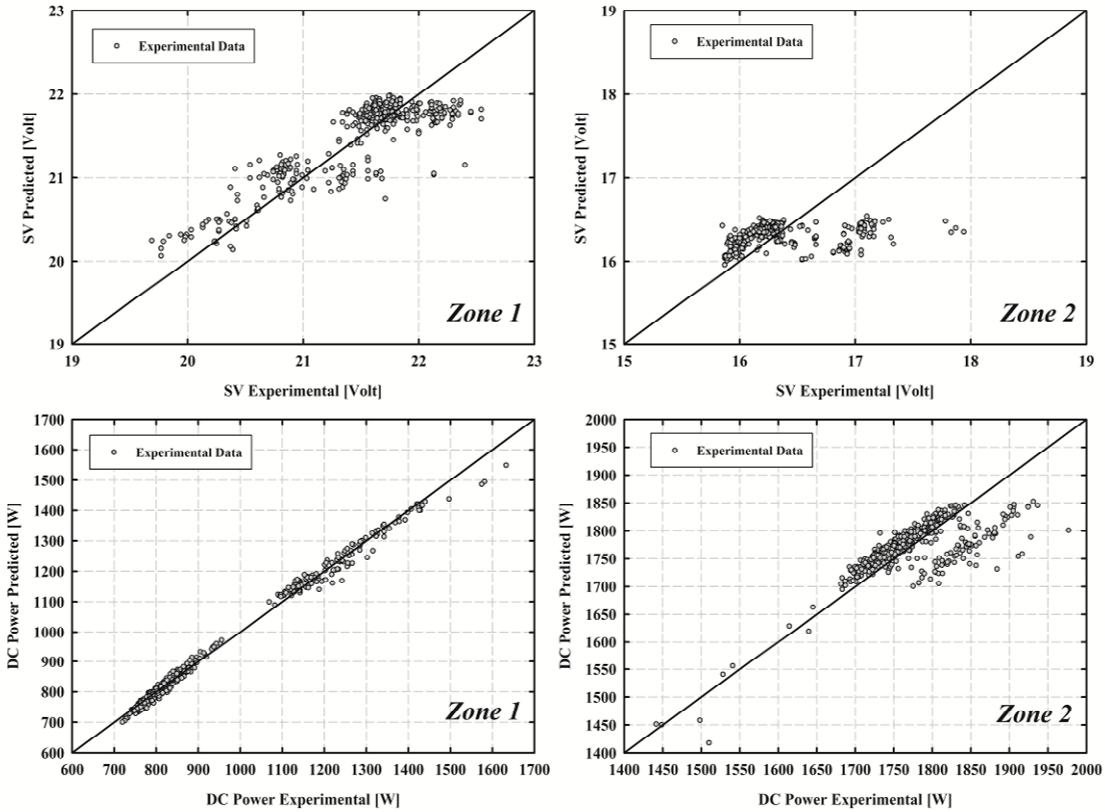

Figure 9. Residuals analysis on SV and DC Power using eqns (1-4)

A two-level FFD was performed within the ranges defined in Table 2 to identify the weight of the single parameters within eqns. (1-4). The purpose of this analysis was to highlight the parameters with the greatest influence on the order of magnitude of SV and DC Power, considering the models derived. The result is contained in the Pareto charts in Figure 10. After screening by means of normal probability plots, It can be seen that the most significant parameters for SV, in absolute terms, for zone 1 are RAirHy>AirF and for zone 2 they are RAirHy>AirF>HyF>DT>TM. So, when the machine operates in the conditions of zone 2, other parameters become important to the machine's performance in terms of SV. Similar conclusion can be drawn observing the Pareto chart relating to DC Power. In zone 1, the order of significance of the parameters, considering their weight in absolute terms, is

SA>AirF>RAirHy>TM>FU, while in zone 2 it is AirF>RAirHy>SA>HyF>DT>TM. In this case, the importance of certain parameters is reversed, and other parameters make their appearance.

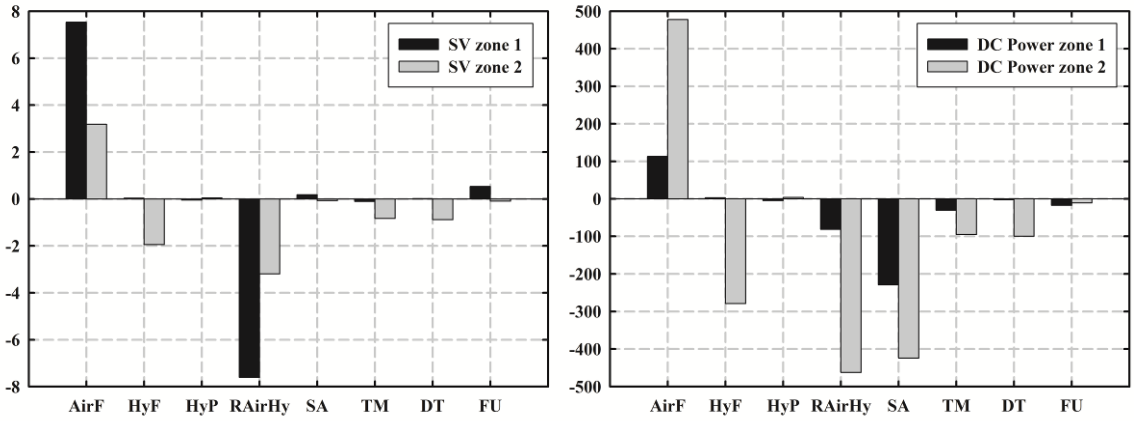

Figure 10. Pareto charts obtained for eqs (1-4)

Obviously the analysis of variance on eqns. (1-4) contain the error from the regression procedure. This means that it is best to focus on the mutual relationships between the weights of the parameters rather than on their absolute values, and also to concentrate just on the parameters that show a higher significance. It would also be possible to avoid the analysis on SV because it could be deducible from the analysis on DC Power. The latter analysis also leads to more reliable results because the correlations derived on DC Power contain a smaller error (Table 6). The analysis on SV nonetheless provides further information on the performance and are more accurate control of the accuracy of the relationships obtained. Finally, the analysis on the equations confirms the results of Table 5, and adds other parameters to those identified in the PCA, which are important for determining the magnitude of SV and DC Power. Considering SA as a variable and consequently excluding SA by the analysis, Figure 10 confirms the importance of the parameters identified in the PCA. In particular, for SV it is obtained:

1) in zone 1, the PCA identifies RAirHy, whereas the FFD identifies AirF and RAirHy as of the parameters with the strongest influence on SV;

2) in zone 2, the PCA identifies just SA as an influential parameter, but SA is an independent variable and so it is implicitly included in the analysis. In other words, SV is *per se* always considered a variable dependent on SA. The FFD thus indicates AirF, HyF and RAirHy as parameters influencing the value of SV. Although they have a high magnitude, TM and DT can be disregarded because their magnitude can be assumed to derive from the regression error.

For DC Power:

1) in zone 1, the PCA points to AirF and RAirHy; the FFD to AirF and RAirHy;

2) in zone 2, the PCA identifies SA, which is excluded from the parameters for the previously mentioned reasons; the FFD suggests AirF, HyF, RAirHy, TM and DT with a smaller influence of TM and DT on the value of DC Power than that of the first three parameters.

It seems clear from the results that the air flow is the main factor used to adjust the unit so as to modulate its performance to suit the required load. As confirmed in [39] the air flow rate can be adjusted to extend the linear correlation between SA and SV even at high currents. The present study demonstrates, however, that when the apparent limiting current is reached, there is a zone in which the correlation between SA and SV is no longer linear. Other operating parameters have to be included in the description of the machine's performance for this zone.

Figure 11 shows the eqns (1-4) applied to a long operating period, also in unsteady states. Although large differences are evident during the start-up, these differences decrease in the transition period between two different steady states of the system. For DC Power the equations (3) and (4) produce very similar values: this is because the parameters with the strongest influence on DC Power in zone 1 also influence zone 2.

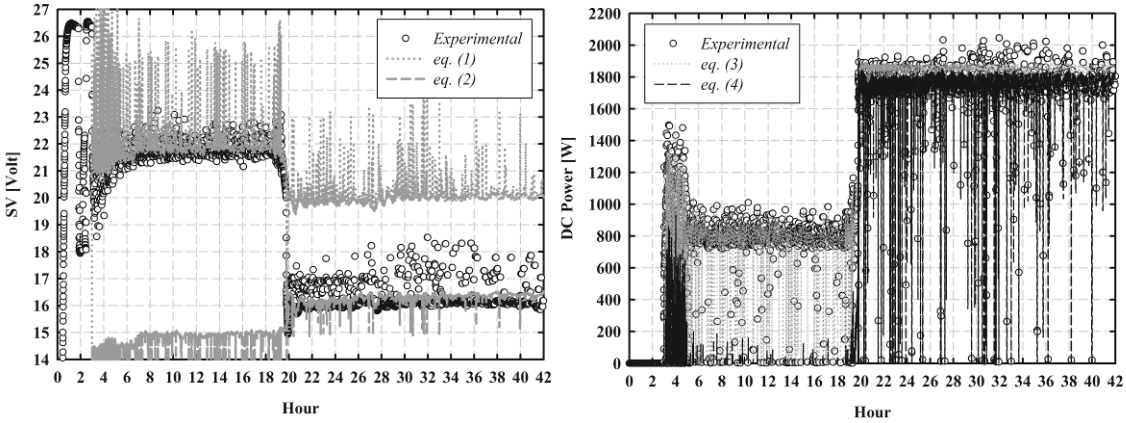

Figure 11. Stack voltage (left) and DC Power (right) during the transition between different steady states

6. Conclusions

This work reports on experimental results obtained in a hydrogen-fueled SOFC electrical generator. Exclusively steady state conditions were investigated. It is difficult to deduce general rules from the data obtained because they consist of a considerable number of quantities that vary simultaneously, also on the basis of control logic installed in the machine. This means that the conclusions that can be drawn are limited. The data collected were typically in the form of arrays of time-dependent values, so graphically representing the relationships between the working variables produced no evident trends, but clusters of points in certain operating regions, which represent different operating conditions. Performing a multivariate analysis on the data produced useful information for interpreting the system as a black box. The analysis conducted enabled us to:

1) cluster the machine's operating data within a limited number of operating conditions;
2) identify the parameters with the strongest influence on SV and DC Power in each operating zone (Table 5 and Figure 10);
3) generate several fairly accurate, progressively simplified multilinear models (contained in Table 6) for predicting the value of SV and DC Power on the basis of the operating parameters estimated directly from input-output data.

In conclusion, the proposed data analysis enabled us to derive general rules that describe the system's operation, and to use said rules to study the system's response to variations in its operating parameters.

7. Acknowledgments

This work was supported by the Italian Ministry for the Environment and the Marche Regional Authority under the CIPE/AERCA project. The authors thank the anonymous reviewers for their insightful comments and precious advice given on how to improve this paper.

8. References

[1] Munch W, Frey H, Edel M, Kessler A. Stationary fuel cells-Results of 2 years of operation at EnBW. J Power Sources 2006;155:77-82.

[2] Gariglio M, De Benedictis F, Santarelli M, Calì M. Analysis of the cooling transient of a large SOFC generator. Int J Hydrogen Energy 2008;33:3204-08.
[3] Gariglio M, De Benedictis F, Santarelli M, Calì M, Orsello G. Experimental activity on two tubular solid oxide fuel cell cogeneration plants in a real industrial environment. Int J Hydrogen Energy 2009;34:4661-68
[4] Raymond AG. Status of tubular SOFC field unit demonstrations. J Power Sources 2000;86:134-9.
[5] Barrera R, De Biase S, Ginocchio S, Bedogni S, Montelatici L. Performance and life time test on a 5kW SOFC system for distributed cogeneration. Int J Hydrogen Energy 2008;33:3193-96
[6] Bassette NF, Wepfer WJ, Winnick J. A Mathematical Model of a Solid Oxide Fuel Cell. J Electrochem Soc 1995;142(11):3792-800.
[7] Chan SH, Khor KA, Xia ZT. A complete polarization model of a solid oxide fuel cell and its sensitivity to the change of cell component thickness. J Power Sources 2001;93:130-40.
[8] Gopalan S, Di Giuseppe G. A macro-level model for determining the performance characteristics of solid oxide fuel cells. J Power Sources 2004;125(2):183-88.
[9] Hernandez-Pacheco E, Singh D, Hutton PN, Patel N, Mann MD. A macro-level model for determining the performance characteristics of solid oxide fuel cells. J Power Sources 2004;138(1-2):174-86.
[10] Bharadwaj A, Archer DH, Rubin ES. Modeling the Performance of a Tubular Solid Oxide Fuel Cell. J Fuel Cell Sci Technol February 2005;2(1):1-7.
[11] Lee KH, Strand RK. SOFC cogeneration system for building applications, part 1: Development of SOFC system-level model and the parametric study. Renewable Energy 2009;34:2831-38.
[12] Qi Y, Huang B, Luo J. Dynamic modeling of a finite volume of solid oxide fuel cell: The effect of transport dynamics. Chem Eng Sci 2006;61:6057-76.
[13] Sunden B, Faghri M. Transport Phenomena in Fuel Cells, Series: Developments in Heat Transfer. first ed. Massachusetts: Boston; 2005.
[14] Erning JW, Hauber T, Stimming U, Wippermann K. Catalysis of the electrochemical processes on solid oxide fuel cell cathodes. J Power Sources 1996;61:205-11.
[15] Shi Y, Cai N, Li C. Numerical modeling of an anode-supported SOFC button cell considering anodic surface diffusion. J Power Sources 2007;164:639-48.
[16] Bessler WG. A new computational approach for SOFC impedance from detailed electrochemical reaction-diffusion models. Solid State Ionics 2005;176:997-1011.
[17] Pakzad A, Salamati H, Kameli P, Talaei Z. Preparation and investigation of electrical and electrochemical properties of lanthanum-based cathode for solid oxide fuel cell. Int J Hydrogen Energy 2010;35:9398-400.
[18] Tsipis EV, Kharton VV. Electrode materials and reaction mechanisms in solid oxide fuel cells: a brief review-I. Performance determining factors. J Solid State Electrochem 2008;12:1039-60.
[19] Santarelli M, Leone P, Calì M, Orsello G. Experimental Activity on a Large SOFC generator. In: Vasquez LO, editor. Fuel Cell Research Trends, Nova Science Publishers Inc; 2007, p. 71-134.
[20] Klein JM, Bultel Y, Pons M, Ozil P. Current and voltage distributions in a tubular solid oxide fuel cell (SOFC). J Appl. Electrochem. 2008;38:497-505.
[21] Oussar Y, Dreyfus G. How to be a gray box model. Neural Networks 2001;14:1161-72.
[22] Abdul-Wahab SA, Bakheit CS, Al-Alawi SM. Principal component and multiple regression analysis in modeling of ground-level ozone and factors affecting its concentrations. Environ Model & Softw 2005;20:1263-71.

[23] King JR, Jackson DA. Variable selection in large environmental data sets using principal components analysis. Envirometrics 1999;10:67-77.
[24] Liu Y, Guo H, Yang P. Exploring the influence of lake chemistry on chlorophyll a: A multivariate statistical model analysis. Ecol Model 2010;221:681-88.
[25] Wahdame B, Candusso D, François X, Harel F, Kauffmann JM, Coquery G. Design of experiment techniques for fuel cell characterisation and development. Int J Hydrogen Energy 2009; 34:967-80.
[26] Lopes VV, Novais AQ, Rangel CM. Hydrogen PEMFC stack performance analysis: A data-driven approach. Int J Hydrogen Energy 2010; 35(18):9973-82.
[27] Placca L, Kouta R, Candusso D, Blachot JF, Charon W. Analysis of PEM fuel cell experimental data using principal component analysis and multi linear regression. Int J Hydrogen Energy 2010;35:4582-91.
[28] Methekar RN, Patwardhan SC, Rengaswamy R, Gudi RD, Prasad V. Experimental evaluation of linear model based control strategies for PEMFCs. Proceedings American Control Conference. St. Louis, MO, USA, 10-12 June 2009;2678-83.
[29] Zhao Y, Ou C, Chen J. A new analytical approach to model and evaluate the performance of a class of irreversible fuel cells. Int J Hydrogen Energy 2008;33:4161-70.
[30] Sammes NM, Du Y, Bove R. Design and fabrication of a 100W anode supported micro-tubula SOFC stack. J Power Sources 2005;145:428-34.
[31] Wang Y, Choi S, Lee E. Fuel cell power conditioning system design for residential application. Int J Hydrogen Energy 2009;34:2340-49.
[32] Jackson JE. A User's Guide to Principal Components. 10 ed. New Jersey: Hoboken; 2003. ISBN 9780471471349.
[33] Khalheim OM. Scaling of analytical data. Anal Chim Acta 1985;177:71-79.
[34] Kishor N, Mohanty SR. Fuzzy modeling of fuel cell based on mutual information between variables. Int J Hydrogen Energy 2010;35(8):3620-31.
[35] Kohonen T. Self-Organizing Maps. 3nd ed. Germany: Berlin; 2001. ISBN 3540679219.
[36] Kahrs O, Brauner N, St. Cholakov G, Stateva RP, Marquardt W, Shacham M. Analysis and refinement of the targeted QSPR method. Comput Chem Eng 2008;32(7):1397-410.
[37] Xu QS, Massart DL, Liang YZ, Fang KT. Two-step multivariate adaptive regression splines for modeling a quantitative relationship between gas chromatography retention indices and molecular descriptors. J Chromatogr A 2003;998(1-2):155-67.
[38] Freni A, Maggio G, Vasta S, Santori G, Polonara F, Restuccia G. Optimization of a solar-powered adsorptive ice-maker by a mathematical method. Solar Energy 2008;82(11):965-76.
[39] Haji S. Analytical modeling of PEM fuel cell i-V curve. Renewable Energy 2011;36:451-58.